Surface and interlayer base-characters in lepidocrocite titanate: The adsorption and intercalation of fatty acid

Tosapol Maluangnont, Pornanan Arsa, Kanokporn Limsakul, Songsit Juntarachairot, Saithong Sangsan, Kazuma Gotoh, Tawan Sooknoi

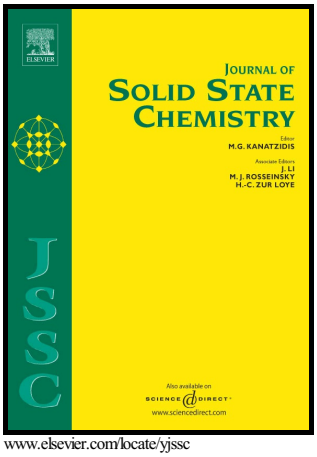

www.elsevier.com/locate/yjssc

PII: S0022-4596(16)30103-7
DOI: http://dx.doi.org/10.1016/j.jssc.2016.03.030
Reference: YJSSC19326

To appear in: *Journal of Solid State Chemistry*

Received date: 31 January 2016
Revised date: 5 March 2016
Accepted date: 18 March 2016

Cite this article as: Tosapol Maluangnont, Pornanan Arsa, Kanokporn Limsakul Songsit Juntarachairot, Saithong Sangsan, Kazuma Gotoh and Tawan Sooknoi Surface and interlayer base-characters in lepidocrocite titanate: The adsorptio and intercalation of fatty acid, *Journal of Solid State Chemistry* http://dx.doi.org/10.1016/j.jssc.2016.03.030

Surface and interlayer base-characters in lepidocrocite titanate: The adsorption and intercalation of fatty acid

Tosapol Maluangnont,*[,†,‡] Pornanan Arsa,[‡,§] Kanokporn Limsakul,[§] Songsit Juntarachairot,[§] Saithong Sangsan,[§] Kazuma Gotoh,[‖] and Tawan Sooknoi*[,‡,§]

[†]College of Nanotechnology, King Mongkut's Institute of Technology Ladkrabang, Bangkok 10520, Thailand

[‡]Catalytic Chemistry Research Unit, Faculty of Science, King Mongkut's Institute of Technology Ladkrabang, Bangkok 10520, Thailand

[§]Department of Chemistry, Faculty of Science, King Mongkut's Institute of Technology Ladkrabang, Bangkok 10520, Thailand

[‖]Graduate School of Natural Science & Technology, Okayama University, 3-1-1 Tsushima-naka, Okayama 700-8530, Japan

*Corresponding author

Email: tosapol.ma@kmitl.ac.th (T.M.); Tel: +66 9 0992 2076; Fax: +66 2 329 8265

Email: kstawan@gmail.com (T.S.); Tel.: + 66 8 1929 8288; Fax: + 66 2 326 4415

Abstract

While layered double hydroxides (LDHs) with positively-charged sheets are well known as basic materials, layered metal *oxides* having negatively-charged sheets are not generally recognized so. In this article, the surface and interlayer base-characters of O^{2-} sites in layered metal oxides have been demonstrated, taking lepidocrocite titanate $K_{0.8}Zn_{0.4}Ti_{1.6}O_4$ as an example. The low basicity (0.04 mmol CO_2/g) and low desorption temperature (50-300^oC) shown by CO_2-TPD suggests that O^{2-} sites at the external surfaces is weakly basic, while those at the interlayer space are mostly inaccessible to CO_2. The liquid-phase adsorption study, however, revealed the uptake as much as 37% by mass of the bulky palmitic acid (C_{16} acid). The accompanying expansion of the interlayer space by ~0.1 nm was detected by PXRD and TEM. In an opposite manner to the external surfaces, the interlayer O^{2-} sites can deprotonate palmitic acid, forming the salt (i.e., potassium palmitate) occluded between the sheets. Two types of basic sites are proposed based on ultrafast ^{1}H MAS NMR and FTIR results. The interlayer basic sites in lepidocrocite titanate leads to an application of this material as a selective and stable two-dimensional (2D) basic catalyst, as demonstrated by the ketonization of palmitic acid into palmitone (C_{31} ketone). Tuning of the catalytic activity by varying the type of metal (Zn, Mg, and Li) substituting at Ti^{IV} sites was also illustrated.

Keyword: Intercalation, layered materials, alkali titanate, basic sites, ketonization, fatty acid

Introduction

Solid base catalysts are capable of activating acidic reactants[1,2] in several reactions of industrial importance, or in the synthesis of fine chemicals[3,4] and first-generation biodiesel.[5] The base-characters of metal oxides originate from under-coordinated O^{2-} sites on different locations (step, corner, terrace, etc.) of the crystals. These sites could behave as the Lewis base by donating an electron pair to reactants. The formation of surface carbonate (or bicarbonate) on oxides in contact to atmospheric CO_2 is an example of the Lewis base-character of oxides. Alternatively, the O^{2-} sites act as the Brønsted base if they abstract a proton from reactants. This is the case for the formation of the surface hydroxyl group on oxides upon contacting with atmospheric water.

Common oxides such as CaO, MgO, ZrO_2 are strongly basic, inexpensive, but typically have low surface area and random distribution of the atomic planes.[6] Their catalytic activity greatly depends on the exposed facets of the crystals which have to be controlled through a delicate synthetic procedure. In contrast, a family of solids known as layered metal oxides/hydroxides [7, 8] naturally crystalizes into two-dimensional (2D) plate-like objects, composed of atomically-thin sheets as elementary units. Such crystals inherently expose the faces (i.e., the basal plane) and the edges to the environment, resulting in the *external* active sites. In addition, the 2D crystals possess the *internal* interlayer space sandwiched between the sheets. These sites can be utilized only if they are accessible to reactants. However, the accessibility to internal basic sites and the thermal/chemical stability do not necessarily coexist in the same catalyst. For example, well-known 2D metal *hydroxides* such as layered double hydroxides (LDHs) or layered hydroxy salts (LHSs) are considered basic largely because they exhibit high affinity toward the acidic molecule CO_2 (in the form of intercalated carbonate CO_3^{2-}), which can have the electrostatic attraction with the positively-charged sheets. However, these

materials transform into (mixed) metal oxides upon contact with reactants at elevated reaction temperature,[8,9,10] thereby losing the two-dimensionality and the associated benefits. Therefore, there is still a need to develop a new type of active and stable 2D solid base catalysts whose the external and the internal surfaces could be effectively utilized.

Lepidocrocite titanates ($A_xM_yTi_{1-y}O_4$, where A = K, M = Zn, Mg, Ni, Cu, Fe^{III}, Mn^{III};[11,12] A = Cs, M = Zn,[13] Ni,[14] Mg,[15,16] Nb;[17] A = K, Rb, and Cs, M = Li;[18,19] A = Cs, M = cationic vacancy[20]) show great potential as thermally stable, 2D basic catalysts. The basal plane (either external or internal) is on the *ac* plane of an orthorhombic unit cell. Two types of bridging basic oxygen atoms can be found. The first one is O_{2c} coordinating to two Ti^{IV} atoms nearby, while the second one is O_{4c} and coordinates to four Ti^{IV} atoms. It is natural to assume that the negative charges on the sheets would localize at O_{2c} and O_{4c}, contributing to the base characters. Moreover, the edges of crystals also contain under-coordinated oxygen atoms of which the exact geometry depends on the extent of hydroxylation. Therefore, the nature of basic sites (O^{2-}) in layered metal oxides is fundamentally different from that in LDHs/LHSs mentioned above. Still, with the exception of a simple ion exchange of interlayer alkali cations with aqueous mineral acids[19,21,22,23, 24,25], reports on base characters of layered metal oxides and their behavior toward other acidic probe molecules are lacking.

In this work, the surface basicity of lepidocrocite titanate $K_{0.8}Zn_{0.4}Ti_{1.6}O_4$ has been characterized by CO_2 temperature programmed desorption (CO_2 TPD). In combination with FTIR and ^1H ultrafast MAS NMR, surface hydroxyl can be revealed. Results were compared to TiO_2 and the well-known basic catalyst such as MgO. Bulky acidic probe molecule, palmitic acid (C_{16} acid), was employed to test the accessibility to the interlayer basic sites via liquid phase adsorption (intercalation). We further demonstrated the application of some lepidocrocite titanates ($K_{0.8}Zn_{0.4}Ti_{1.6}O_4$, $K_{0.8}Mg_{0.4}Ti_{1.6}O_4$ and $K_{0.8}Li_{0.27}Ti_{1.73}O_4$) as catalysts for the gas-phase

ketonization of palmitic acid, in comparison to the mixed Mg/Al oxides from the decomposition of LDH. The ketonization of carboxylic acids to the respective ketones is of industrial importance as a processing step in biomass conversion to hydrocarbon fuels.[26, 27, 28, 29]

Material and Methods

Synthesis. Lepidocrocite titanate $K_{0.8}Zn_{0.4}Ti_{1.6}O_4$ was synthesized[11] by the calcination of the stoichiometric mixture of K_2CO_3, ZnO, and TiO_2 at 900ºC for 20 h. Two other compositions, $K_{0.8}Mg_{0.4}Ti_{1.6}O_4$ and $K_{0.8}Li_{0.27}Ti_{1.73}O_4$, can be prepared similarly but replacing ZnO with MgO[11] and Li_2CO_3,[18,19] respectively. The layered double hydroxide with Mg/Al mole ratio of 2.5 was synthesized by a coprecipitation method[30] and was calcined at 450 ºC for 6 h, giving the mixed Mg/Al oxide "MgAl2.5". Potassium palmitate was obtained as the white powder from the reaction between KOH(aq) and palmitic acid. The PXRD patterns of other materials in addition to $K_{0.8}Zn_{0.4}Ti_{1.6}O_4$ can be found in Figure S1-S2 in Supporting Information. All chemicals are of reagent grade and were used as received, except K_2CO_3, Li_2CO_3, KOH and palmitic acid which were dried 120ºC overnight prior to use.

CO_2 temperature programmed desorption. Approximately 200-300 mg of the sample was activated in situ at 450ºC for 2 hours under air zero in a quartz tube reactor, followed by a cooling to room temperature under N_2 gas. Gaseous CO_2 was then flown through the sample at the flow rate 30 mL/min for an hour, followed by a flow of helium at the same flow rate for another hour. Next, the temperature was raised from room temperature to 600ºC at 5ºC/min using pure helium as a carrier gas. The CO_2 desorption profile was recorded by a thermal conductivity detector and was normalized by mass of the sample employed. The basicity was expressed as mmol of CO_2 per g of the sample. The peak area obtained was compared to that from a known

amount of $CaCO_3$ which decomposes completely and quantitatively to CaO and CO_2. All gases are the commercial products of Praxair with the purity of 99.99% and were used as received.

Adsorption of palmitic acid. An amount of 2.0 g of $K_{0.8}Zn_{0.4}Ti_{1.6}O_4$ was heated with 150 mL of a 5%w/w palmitic acid (Fluka, 97%+) in isopropanol at 60ºC from 1 to 36 h. The liquid was withdrawn at certain intervals, and the content of adsorbed palmitic acid was determined based on equation (1), together with an appropriate conversion of concentration to mass. Here, A_0 is the corrected peak area of palmitic before the adsorption, and A_t is the corrected peak area of palmitic acid remaining in the mother liquor after the adsorption time *t*.

$$\%\text{Adsorption} = [(A_0-A_t)/A_0]\times 100\% \quad (1)$$

The solid was filtered, washed with isopropanol, and then dried at 70ºC overnight. The experiment with decanoic acid was performed similarly. A control experiment was performed by heating $K_{0.8}Zn_{0.4}Ti_{1.6}O_4$ with isopropanol at 60 ˚C in the absence of any carboxylic acid. Another control experiment was also performed, where $K_{0.8}Zn_{0.4}Ti_{1.6}O_4$ was magnetically stirred with 1 M HCl (3 times, 12 h each, with the fresh HCl loaded between repetition)[24] so as to obtain the proton-containing lepidocrocite where K^+ is ion exchanged with $H^+\cdot H_2O$.

Characterization. Powder X-ray diffraction (PXRD) measurements were conducted on a Rigaku DMAX 2200/Ultima+ diffractometer, employing a Cu-Kα radiation at 40 kV and 30 mA. The sample was scanned in the range 2θ = 5-65º at a 0.05 degree/step and a detection time of 0.6 second/step. BET specific surface area of the sample was determined by a Gas Adsorption Analyzer (Autosorb-1C, Quantachrome). For TGA (Perkin-Elmer, Pyris 1), the sample was heated from room temperature to 900ºC (10ºC/min) under nitrogen gas flowing at 20 mL/min. FTIR spectra of the pelletized samples (prepared by grinding with KBr) were collected on a

Spectrum GX (Perkin Elmer) spectrometer. SEM images were acquired on a Zeiss EVO/MA10 scanning electron microscope, while TEM images were acquired on a JEOL JEM 2010 transmission electron microscope. ^{1}H MAS NMR (spinning speed: 100 kHz) of $K_{0.8}Zn_{0.4}Ti_{1.6}O_4$ was recorded using a JEOL ECA-600 spectrometer with a 0.75 mmϕ MAS sample rotor. Depth2 pulse sequence with 1.3 μs of 90° pulse length and 5.0 s of repetition time were applied to obtain a spectrum.

Catalytic activity testing. Catalytic activity testing was conducted in a continuous fixed bed down-flow reactor made of glass (length, 50 cm; outer diameter, 8 mm; inner diameter, 6 mm) under atmospheric pressure of N_2. The catalyst was activated to 800^{o}C in air zero for an hour, followed by a cooling to the reaction temperature (375^{o}C) under air zero. Then, 5% palmitic acid in *p*-xylene was fed into the reactor by an HPLC pump at a flow rate of 0.025 mL/min. The catalyst activity testing was conducted at atmospheric pressure, at the contact time (*W/F*) of 1500 g·h/mol, and the flow rate of palmitic acid plus carrier gas (N_2) of 30 mL/min, for a total of 360 min. The liquid products were trapped by an ice bath and collected every 45 minutes before the analysis by an HP6890 gas chromatograph (Hewlett-Packard). The catalyst recovered after the activity testing at the mentioned condition is hereafter called "spent".

Results and discussion

Calcination of the stoichiometric mixture of K_2CO_3, ZnO, and TiO_2 at 900ºC for 20 h results in the lepidocrocite titanate $K_{0.8}Zn_{0.4}Ti_{1.6}O_4$ with high crystallinity, as shown by the PXRD pattern in Figure 1a. This product will be hereafter called "as made" $K_{0.8}Zn_{0.4}Ti_{1.6}O_4$. The diffraction pattern can be indexed based on the orthorhombic symmetry, with unit cell parameters (refined by Cellcalc) of a = 0.3809(3), b = 1.567(1), and c = 0.2981(2) nm, in agreement with the previous work (suggested space group[11] $Cmc2_1$). The first peak at 2θ = 11.34º (d = 0.78 nm) corresponds to the 020 reflection which is the repeating distance of the edge-shared TiO_6 (or $(Ti/Zn)O_6$) sheets stacking along the *b*-direction. Figure 2a shows that the plate-like crystals of the as made $K_{0.8}Zn_{0.4}Ti_{1.6}O_4$ with the lateral size up to 2 μm × 2 μm form aggregates, likely due to the use of high temperature in the synthesis. $K_{0.8}Zn_{0.4}Ti_{1.6}O_4$ had an extremely low specific surface area of 3 m^2/g.

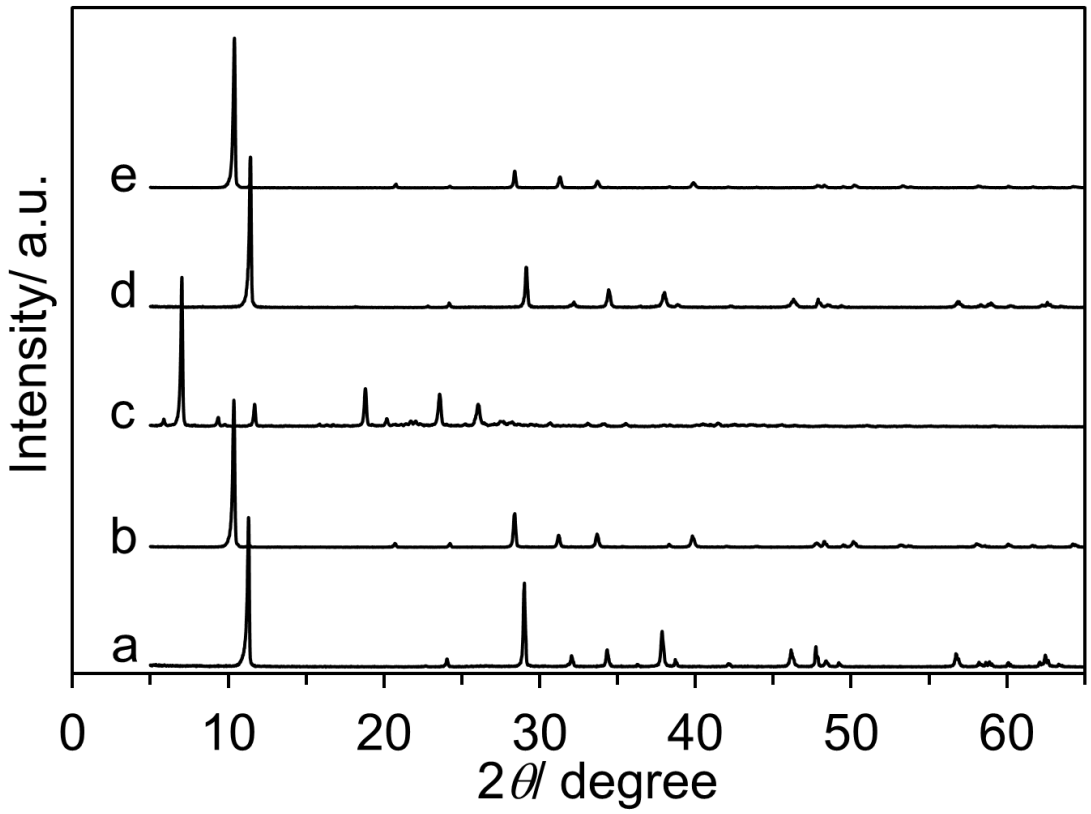

Figure 1. PXRD patterns of (a) as made $K_{0.8}Zn_{0.4}Ti_{1.6}O_4$, (b) the solid product after the adsorption of the 5%w/w palmitic acid/isopropanol solution at 60^{o}C for 36 h, (c) potassium palmitate, (d) the solid product heated with isopropanol only, and (e) similar to (b) but with decanoic acid.

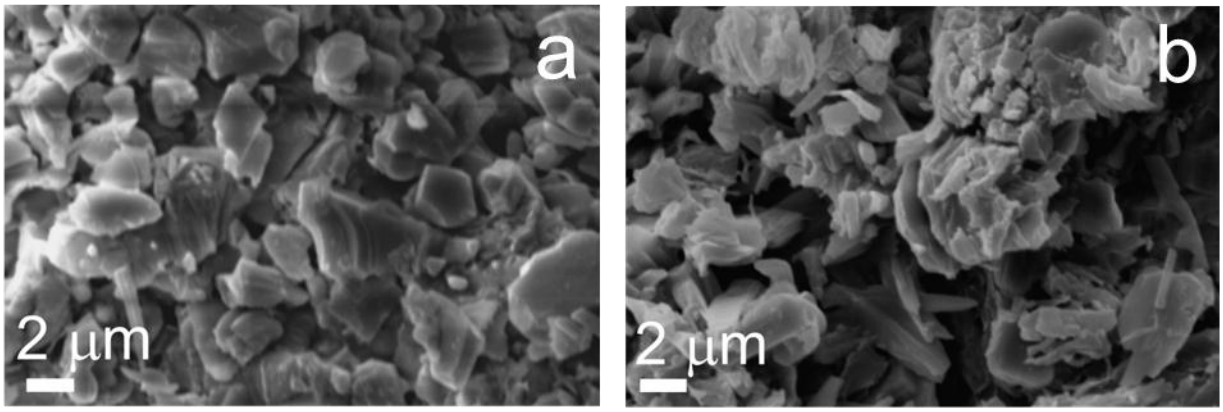

Figure 2. SEM images of (a) as made, and (b) spent $K_{0.8}Zn_{0.4}Ti_{1.6}O_4$.

The CO_2 desorption profiles of $K_{0.8}Zn_{0.4}Ti_{1.6}O_4$ and other tested materials are shown in Figure 3. CO_2 desorbs from $K_{0.8}Zn_{0.4}Ti_{1.6}O_4$ in the range 50-300ºC (with the peak temperature T_p at 89ºC), which is close to the range reported for mixed sodium/potassium titanate nanotubes.[31] A relatively low T_p suggests that the majority of CO_2 adsorption occurrs physically. Lepidocrocite titanate $K_{0.8}Zn_{0.4}Ti_{1.6}O_4$ is therefore a relatively weak base solid, similar to other reported titanate-based materials.[31, 32] On the other hand, CO_2 desorption from TiO_2 anatase (T_p = 120ºC) and "MgAl2.5", which is the mixed (Mg/Al) oxide from the decomposition of layered double hydroxide (T_p = 170ºC), span a wider range (both in the range 50-400ºC). CO_2 molecules adsorbed on these two materials could contain a minor fraction which was adsorbed chemically, in addition to the major fraction which was adsorbed physically. While MgO shows the small peak at T_p = 196ºC somewhat similar to $K_{0.8}Zn_{0.4}Ti_{1.6}O_4$, TiO_2 and MgAl2.5, a very strong CO_2 desorption at 400-700ºC is due to the decomposition of $MgCO_3$ which was produced *in situ* from the exposure of MgO to CO_2. The strength of the basic sites which are accessible to CO_2 can be estimated from T_p, and is in the order: $K_{0.8}Zn_{0.4}Ti_{1.6}O_4$ < TiO_2 < MgAl2.5 < MgO.

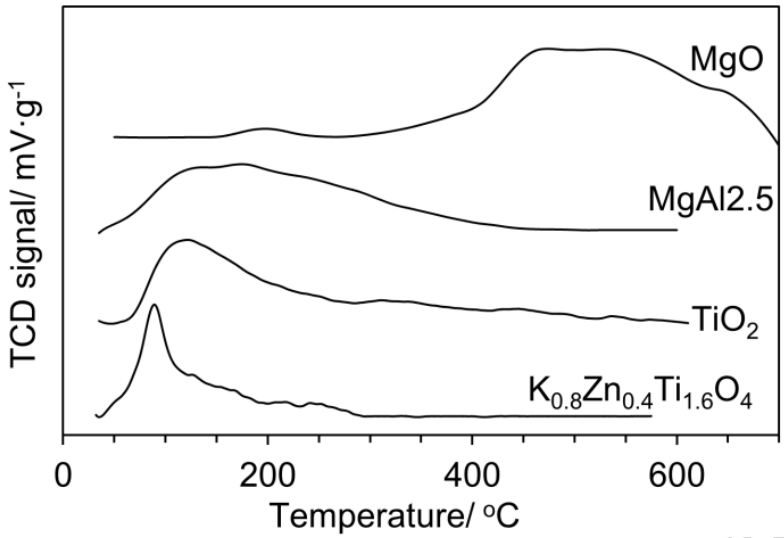

Figure 3. CO_2 desorption profiles of as made $K_{0.8}Zn_{0.4}Ti_{1.6}O_4$, TiO_2 (anatase), MgAl2.5 which is a mixed (Mg/Al) oxide from the decomposition of a layered double hydroxide with Mg/Al = 2.5, and MgO. The y-axis is the signal from the thermal conductivity detector normalized by the mass of the sample.

The basicity (mmol CO_2/g, in parenthesis) is in the order: $K_{0.8}Zn_{0.4}Ti_{1.6}O_4$ (0.04) < TiO_2 (0.07) < MgAl2.5 (0.82) < MgO (1.18). Excluding MgO whose the CO_2 desorption has a contribution from the bulk, these values parallel the surface area (m^2/g) of each material which is in the order $K_{0.8}Zn_{0.4}Ti_{1.6}O_4$ (3) < TiO_2 (6) < MgAl2.5 (122). Our results imply the inaccessibility of the O^{2-} sites at the interlayer region of $K_{0.8}Zn_{0.4}Ti_{1.6}O_4$ with respect to gaseous CO_2. Consequently, the adsorption of CO_2 should take place at the sites located on the external surfaces of the crystals only. It is important to note that CO_2-TPD detects the basic sites accessible by CO_2 without discriminating whether they are O^{2-} or OH sites. These basic sites could react with CO_2, forming carbonate (for O^{2-}) or bicarbonate (for OH) in various configurations.[33] Interestingly, the basicity of $K_{0.8}Zn_{0.4}Ti_{1.6}O_4$ (0.04 mmol/g) with a low surface area of 3 m^2/g is just slightly different from some of the values reported for titanate nanotubes

(0.03-0.05 mmol/g)[31] despite a much larger surface area of the nanotubes (generally more than 100 m^2/g).[31]

The FTIR spectrum of $K_{0.8}Zn_{0.4}Ti_{1.6}O_4$ is shown in Figure 4a. The sharp peak at 811 cm^{-1} is due to Ti-O lattice vibration.[18,19] For comparison, the peak at 899 cm^{-1} was reported[34] and assigned similarly in a lepidocrocite titanate with interlayer Na^+ cations. The band at 3418 and 1624 cm^{-1} can be ascribed to the stretching and bending vibration of adsorbed H_2O[18,19] respectively. The hydroxyl group attached to the layered titanates can be found generally at 900-1000 cm^{-1}.[18, 19, 35, 36, 37] It is likely that the sharp peak at 1018 cm^{-1} in $K_{0.8}Zn_{0.4}Ti_{1.6}O_4$ (Figure 4a) has similar origin. The relatively high wavenumber of this peak in relation to others[18, 19, 35, 36, 37] suggests a strong bonding between the oxygen atom (i.e., O^{2-} sites) and the hydrogen atom (presumably from adsorbed water molecules). In addition to the formation of a hydroxylated surface, a small band at 1388 cm^{-1} due to the asymmetric stretching of monodentate carbonate (vs 1378 cm^{-1} as calculated by Mino et al.[38]) can be observed. Here, the O^{2-} sites are the Lewis basic donating an electron pair to gaseous CO_2 in the atmosphere. Other peaks at ~2300-2375 cm^{-1} are due to the asymmetric stretching of gaseous CO_2. Several bands at 2850-3000 cm^{-1} are due to CH stretching of the thin organic films coated on an FTIR window.

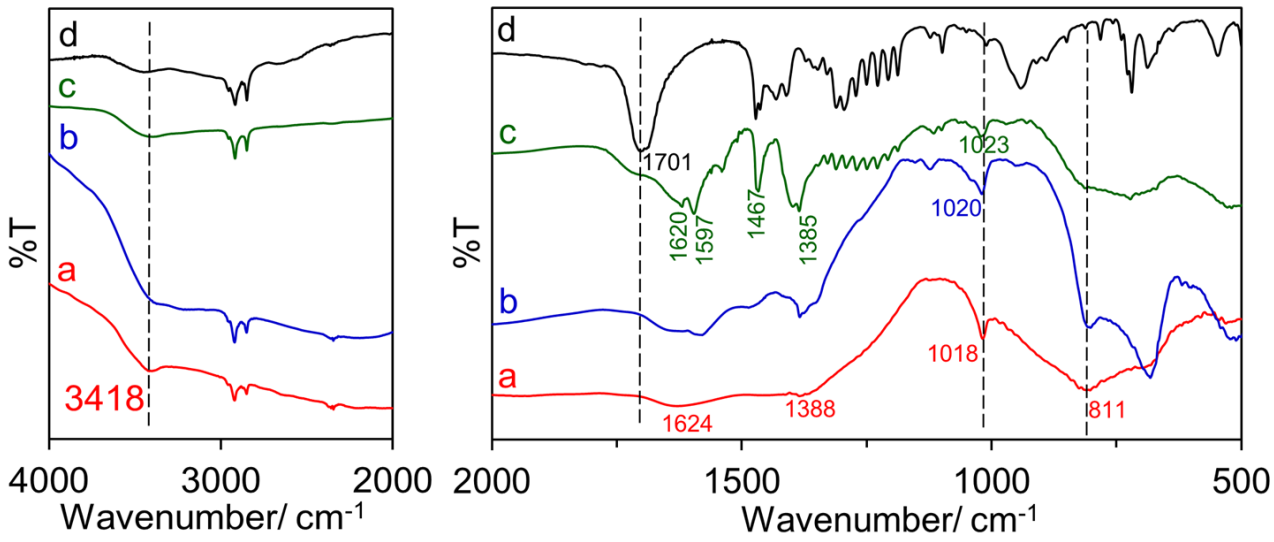

Figure 4. FTIR spectrum of (a) as made $K_{0.8}Zn_{0.4}Ti_{1.6}O_4$, (b) the solid product after being heated with isopropanol only, (c) the solid product after the adsorption of the 5%w/w palmitic acid/isopropanol solution at 60°C for 36 h, and (d) palmitic acid.

The solid state ^1H ultrafast MAS NMR spectrum of as made $K_{0.8}Zn_{0.4}Ti_{1.6}O_4$ is shown in Figure 5. The peak at 4.1 ppm (FWHM = 0.6 ppm) is assigned to protons of physisorbed water.[39, 40] The presence of water molecules as detected by NMR agrees with results by FTIR just mentioned. The broad signal at ~9 ppm can be deconvoluted into two peaks at 8.2 and 9.0 ppm (FWHMs of both peaks are 2.0 ppm), suggesting that these two protons are in very similar yet different chemical environments. These signals can be inferred to water molecules interacting with two types of O^{2-} sites in as made $K_{0.8}Zn_{0.4}Ti_{1.6}O_4$. Since there are two types of structural oxygen atoms, each bound to different number of Ti^{IV} atoms, two partially overlapped H signals could be expected. For comparison, the peaks at 7.9 and 10.0 ppm have been reported in protonated titanate nanotubes,[41] and at 6.0 and 8.0 ppm in $H_2Ti_3O_7$.[42] However, in these materials[41,42] the signals are due to protons introduced via acid ion exchange, while in our case

the presence of protons (or hydroxyl groups) is most likely a result of the affinity between O^{2-} sites and atmospheric water.

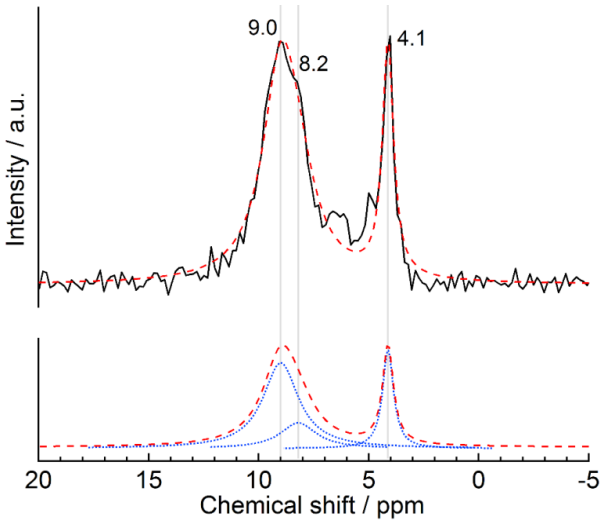

Figure 5. ^{1}H MAS NMR spectrum of as made $K_{0.8}Zn_{0.4}Ti_{1.6}O_4$ (black solid line) and the fitting spectrum (red broken line). The deconvoluted Lorentzian components are shown by blue dotted lines at the bottom spectrum.

In order to demonstrate the accessibility of interlayer basic sites, we performed a liquid-phase adsorption study of a 5% w/w palmitic acid in isopropanol on as made $K_{0.8}Zn_{0.4}Ti_{1.6}O_4$ at 60^{o}C. As shown in Figure 6, the uptake of "palmitic acid" gradually increases to 34.5% (12 h) by weight, and remains constant after that (34.9%, 36 h). Such a large adsorption *solely* to the external surfaces is unlikely considering the extremely low surface area of 3 m^2/g. Instead, the internal surfaces must involve in this uptake. We will show later on that "palmitic acid" is adsorbed as palmitate species, and that the adsorption involves the interlayer space, i.e., intercalation. In agreement with %adsorption determined from the mother liquor, the solid after contact with palmitic acid at 36 h shows 37.0% mass loss in the range 200-400^{o}C (Figure 7a), ascribed to the loss of the adsorbed "palmitic acid". The mass loss curve of palmitic acid is shown for comparison in Figure 7c. Besides, Figure 7b shows a negligible mass loss from the

control experiment in the absence of palmitic acid where only isopropanol was in the liquid phase.

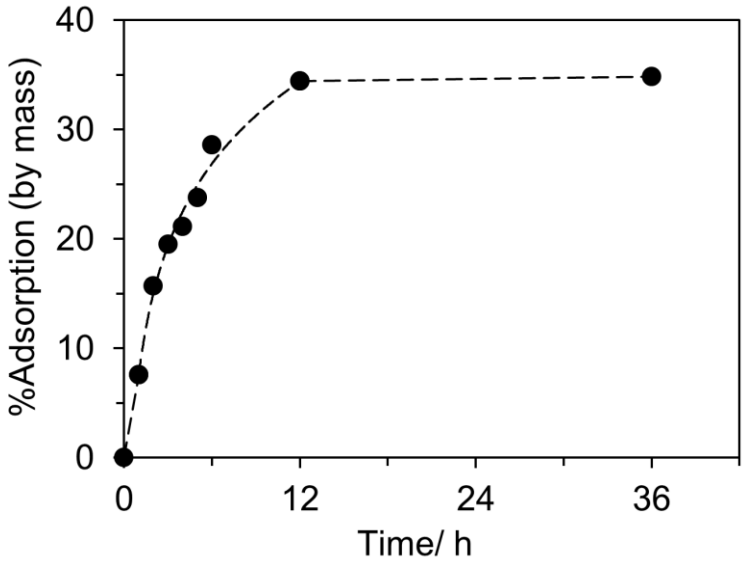

Figure 6. The %adsorption by mass of palmitic acid by $K_{0.8}Zn_{0.4}Ti_{1.6}O_4$ at 60°C, determined from the corrected peak area of palmitic acid before the adsorption (A_0) and at time t (A_t) of the mother liquor.

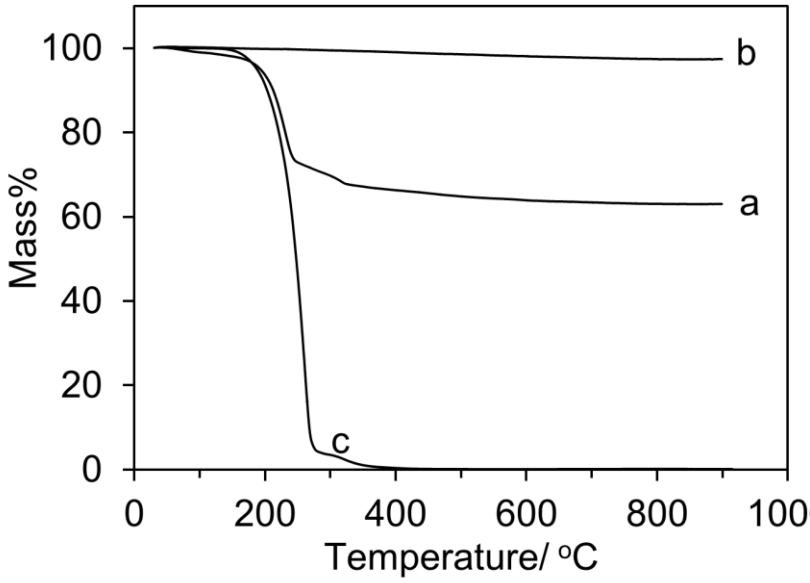

Figure 7. Mass loss curves of (a) the solid product after the adsorption of the 5%w/w palmitic acid/isopropanol solution to $K_{0.8}Zn_{0.4}Ti_{1.6}O_4$ at 60°C for 36 h, (b) the solid product treated with isopropanol only, and (c) palmitic acid.

In line with above view, PXRD pattern of the sample after palmitic acid adsorption in Figure 1b shows an expansion of the interlayer. The PXRD pattern can also be indexed based on the orthorhombic symmetry, but with a = 0.3763(1) nm, b = 1.7190(7) nm, and c = 0.3005(1) nm. While the orthorhombic unit cell of pristine $K_{0.8}Zn_{0.4}Ti_{1.6}O_4$ is C based-centered[11] (hkl reflections observed following h+k = 2n), such restriction is no longer hold considering the presence of reflections such as 121, 141, 161, 211 and 251. Instead, the unit cell of this product is likely primitive orthorhombic. (See also Figure S3 and Table S1.) Unfortunately, the quality of the data does not allow us to do Rietveld analysis. Two parameters (a and c) are close to those in as made $K_{0.8}Zn_{0.4}Ti_{1.6}O_4$, suggesting that the host layer was kept unchanged during the adsorption. The most obvious feature is the shift of the first peak (i.e., d_{020}) to a lower angle 2θ = 10.36° (i.e, larger spacing d = 0.85 nm), resulting from the expansion of ~0.1 nm. While this

expansion is rather small compared to typical values (0.3-0.4 nm) reported[43, 44] for the intercalation compounds having an alkyl chain, the 0.23 nm-expansion due to the pressure-induced intercalation[45] of ethanol into $K_{0.8}Ni_{0.4}Ti_{1.6}O_4$ has been reported. For comparison, the unit cell parameters a = 0.378(3) nm, b = 1.79(2) nm, and c = 0.298(4) nm can be deduced from the PXRD pattern (Figure S4) of the proton-containing solid prepared via repeated ion exchange with aqueous HCl. The relatively large d spacing (d_{020} = 0.90 nm at $2\theta = 9.82^o$) is due to the intercalation of $H^+ \cdot H_2O$ in agreement with the literature,[46] but is in sharp contrast to the small d_{020} in Figure 1b.

In $K_{0.8}Zn_{0.4}Ti_{1.6}O_4$ having the C based-centered unit cell (space group $Cmc2_1$),[11] potassium cations sit at the 4a site within the trigonal prismatic cavity. Since the two adjacent sites are too small to be occupied simultaneously, the site occupancy[11] of only 40% was achieved. So, there are rooms available for the subsequent intercalation of the guest species into the interlayer space. Upon intercalation, we observed the change of the symmetry from C-base centered to the primitive one. Recently, Shirpour et al.[47] have reported a similar change as $K_{0.8}Li_{0.27}Ti_{1.73}O_4$ intercalates the bulky *hydrated* sodium cations. This change occurs via the lateral gliding of the lepidocrocite layers along the a axis by a/2, generating a relatively larger cubic cavity for the guest species. Based on this cited work[47], we propose that the cubic cavity could *locally* accommodate palmitic acid (palmitate) while limiting the long-range expansion along the b-direction. It could be deduced that the strong guest-host interaction (i.e., acid-base interaction between palmitic acid and O^{2-} sites) overcomes the weaker host-host interactions such that the gliding of the layers is possible. Other examples[18,45,48] of the change of symmetry of the orthorhombic unit cell in lepidocrocite titanate upon the intercalation of guest species have also been reported.

The PXRD pattern of the solid product heated with isopropanol only (Figure 1d) is similar to that of the as made $K_{0.8}Zn_{0.4}Ti_{1.6}O_4$, suggesting the essential role of palmitic acid in such topotactic transformation. The FTIR spectrum of the isopropanol-treated $K_{0.8}Zn_{0.4}Ti_{1.6}O_4$ in Figure 4b is generally similar to as made $K_{0.8}Zn_{0.4}Ti_{1.6}O_4$, with some variations in the relative peak intensities. We also exclude the possibility that the expanded product be potassium palmitate, as evidenced from the notable differences between Figure 1c and Figure 1b. Additionally, replacing palmitic acid ($C_{15}H_{31}COOH$) by decanoic acid ($C_9H_{19}COOH$) gave the product with a similar PXRD pattern (Figure 1e) and unit cell parameters (a = 0.3760(4) nm, b = 1.716(2) nm, and c = 0.3002(3) nm). The similar interlayer spacing in these two cases suggests the orientation where the long molecular axis of the acids is parallel to inorganic sheets.

Further evidence for the interlayer expansion is the TEM image. It can be seen that as made $K_{0.8}Zn_{0.4}Ti_{1.6}O_4$ shows a repeating distance of ~0.8-0.9 nm (Figure 8a), while the solid after the adsorption of palmitic acid exhibits a repeating distance of ~1.0 nm (Figure 8b). These distances agree reasonably with the d-spacing of the first peak in the respective PXRD patterns.

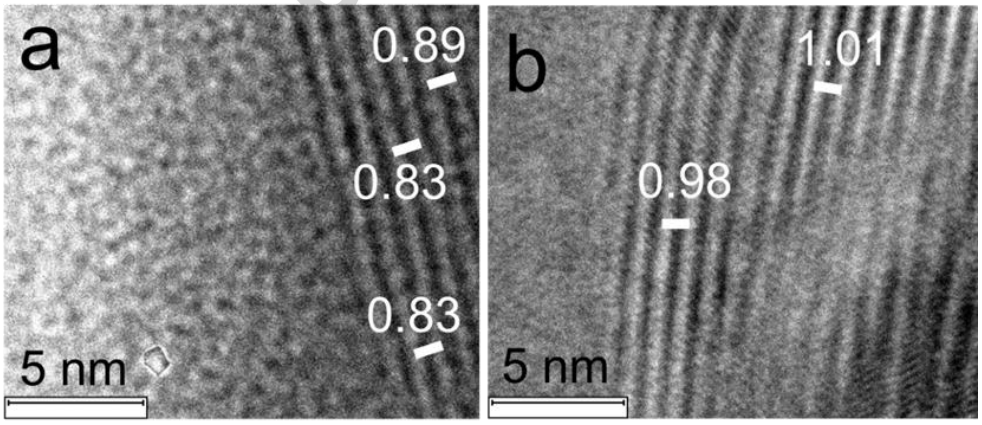

Figure 8 TEM images of (a) as made $K_{0.8}Zn_{0.4}Ti_{1.6}O_4$, and (b) the solid product after adsorption of palmitic acid at 60°C for 36 h.

The characteristics peaks in the FTIR spectrum of palmitic acid in Figure 4d include the strong C=O stretching at 1701 cm^{-1}, and the OH stretching at 3420 cm^{-1}. The co-presence of these two peaks is widely accepted as the signature of a carboxylic acid. Several other peaks serve as a fingerprint especially at 1000-1250 cm^{-1}. Unfortunately, the peaks due to CH_2 symmetric and asymmetric stretching (~2850-2960 cm^{-1}) overlap with the thin organic films coated on the FTIR window. Interestingly, while the OH stretching is still visible, the C=O stretching is very weak in $K_{0.8}Zn_{0.4}Ti_{1.6}O_4$ refluxed with palmitic acid (Figure 4c). Instead, the peaks at 1597 and 1385 cm^{-1} were detected and assigned to the asymmetric and symmetric stretching of the carboxylate anion,[49] respectively. These results suggest the existence of *palmitate species*. Besides, two other peaks (1620 and 1467 cm^{-1}) at the positions slightly shifted from the previous ones (1597 and 1385 cm^{-1}) indicate that palmitate species are in two environments. Several vibrations in the range 1000-1250 cm^{-1} are maintained, confirming the integrity of the skeleton of the intercalated palmitate species after the intercalation into $K_{0.8}Zn_{0.4}Ti_{1.6}O_4$.

Basic sites at several positions in $K_{0.8}Zn_{0.4}Ti_{1.6}O_4$ crystals might involve in the uptake of palmitic acid. Initially, palmitic acid would be adsorbed onto the external basic sites at the basal plane or the edges. The adsorption at the latter site might specifically lead to the rearrangement/activation of palmitic acid into the geometry suitable for the subsequent intercalation *into* the interlayer region. The internal O^{2-} sites at the interlayer region act as a Brønsted base, abstracting the proton from palmitic acid. Meanwhile, the charge-balancing potassium cations at the interlayer region migrate close to the newly-formed palmitate anion, so as to preserve charge neutrality of the system as shown by equation (2):

$$K_{0.8}[Zn_{0.4}Ti_{1.6}O_4] + 0.8C_{15}H_{31}COOH \rightarrow H_{0.8}[Zn_{0.4}Ti_{1.6}O_4] + 0.8C_{15}H_{31}COOK \qquad (2)$$

where the species in the bracket represents the immobilized layers of lepidocrocite titanate. This reaction might be driven by the acid-base interactions between interlayer O^{2-} sites and proton of palmitic acid, and also by the electrostatic attraction between palmitate anion and K^+. Our observation is somewhat different from that reported [50] by Chou et al., where only the complexation of the carboxylate with divalent (but not monovalent) cations in smectite clays drives the formation of the occluded salt. Upon the intercalation, an internal hydroxylated surface would be formed, together with the palmitate species. The peak at 1023 cm^{-1} in Figure 4c could be the O-H stretching of the hydroxyl group attached to the layered titanates, similar to the one in as made $K_{0.8}Zn_{0.4}Ti_{1.6}O_4$ at 1018 cm^{-1}. According to equation (2), and using the formula mass of 198.02 g/mol ($K_{0.8}Zn_{0.4}Ti_{1.6}O_4$) and 256.42 g/mol (palmitic acid), the content of fully intercalated palmitic acid would be as high as $[(0.8\times256.42)/(198.02 + 0.8\times256.42)]\times100\% = 50.9\%$. So, it is reasonable that the uptake of 37% from GC analysis and TGA (Figure 6 and 7) virtually originates from the "palmitic acid" adsorbed at the interlayer space of this material.

The fact that $K_{0.8}Zn_{0.4}Ti_{1.6}O_4$ intercalates carboxylic acids into the interlayer space has prompted us to investigate its use as a catalyst in the gas-phase ketonization of palmitic acid. The removal of oxygen atom by ketonization (i.e., the transformation of two molecules of the acid into the ketone) could be coupled with the cracking of the corresponding ketone to C_{10} to C_{14} hydrocarbons applicable for use as a diesel fuel. Table 1 compares the conversion of palmitic acid and the distribution of products obtained over tested materials. The 86% conversion of palmitic acid was achieved over $K_{0.8}Zn_{0.4}Ti_{1.6}O_4$, giving palmitone $C_{15}H_{31}(C=O)C_{15}H_{31}$ as the major product via ketonization process. Other groups of products include heavy ketone (mostly C_{17} ketone $CH_3(C=O)C_{15}H_{31}$), C_{10} to C_{14} hydrocarbons, and light hydrocarbons ($<C_{10}$). These products were formed via the cracking at the α,β-position of palmitone, followed by further cracking and/or hydrogen transfer. A detailed reaction pathway for the formation of these

products is under investigation and will be reported in a near future. Figure S5 shows the PXRD pattern of spent $K_{0.8}Zn_{0.4}Ti_{1.6}O_4$, confirming that the lepidocrocite structure is preserved under the heat treatment in air at 800ºC and subsequent contact with palmitic acid at 375ºC (see Experimental section). The stability of $K_{0.8}Zn_{0.4}Ti_{1.6}O_4$ is in contrast to other layered materials such as layered double hydroxide (LDH)[9] or layered hydroxy salt (LHS)[10] which undergo structural transformation upon contact with liquid fatty acids at 100-140ºC. We also tested the catalytic activity of the mixed (Mg/Al) oxide "MgAl2.5", which is known to catalyze the ketonization of carboxylic acids by its basic sites.[51, 52, 53] MgAl2.5 gave an almost complete conversion of palmitic acid with a smaller yield of palmitone (36%, vs 59% over $K_{0.8}Zn_{0.4}Ti_{1.6}O_4$), together with the larger yield of hydrocarbon products.

Table 1. Conversion of palmitic acid and the distribution of liquid products over three compositions of lepidocrocite titanate and MgAl2.5.[a]

Catalyst	$K_{0.8}Zn_{0.4}Ti_{1.6}O_4$	$K_{0.8}Mg_{0.4}Ti_{1.6}O_4$	$K_{0.8}Li_{0.27}Ti_{1.73}O_4$	MgAl2.5
Conversion	85.6	96.5	97.9	96.9
Product distribution				
Palmitone	58.6	41.5	39.2	35.5
Heavy ketone[b]	7.1	28.1	23.4	37.0
C_{10} to C_{14} hydrocarbons	17.7	26.5	34.5	22.6
Light hydrocarbons	1.0	1.0	2.9	5.0

[a] Reaction conditions: 5% palmitic acid in *p*-xylene; flow rate of feed plus carrier gas (N_2) 30 $mL \cdot min^{-1}$; reaction temperature 375ºC, atmospheric pressure; W/F = 1500 g·h/mol. The values shown were averaged at the time on stream 225-360 min where conversion and product distributions were stabilized.

[b] C_{17} ketone $CH_3(C{=}O)C_{15}H_{31}$ and others

Besides, an almost complete conversion of palmitic acid over two other compositions of lepidocrocite titanate was obtained (Table 1). This result can be explained by their larger specific surface area ($K_{0.8}Mg_{0.4}Ti_{1.6}O_4$, 13 m^2/g; $K_{0.8}Li_{0.27}Ti_{1.73}O_4$, 28 m^2/g), among several factors. Since the adsorption of palmitic acid must take place initially before subsequent diffusion and activation at the interlayer space, the catalysts with higher surface area would facilitate the latter two processes. The increase in palmitic acid conversion over these two catalysts is hence accompanied by a decrease in the yield of palmitone, as compared to that over $K_{0.8}Zn_{0.4}Ti_{1.6}O_4$. Yet, the yields of hydrocarbons over Mg and Li-containing lepidocrocite titanate (26-34%) are higher than those over MgAl2.5 (22%). This result indicates a better selectivity of Mg- and Li-containing lepidocrocite titanate toward cracked hydrocarbons, as compared to typical basic oxides.

The high conversion (86%) of palmitic acid over $K_{0.8}Zn_{0.4}Ti_{1.6}O_4$ with a low specific surface area (3 m^2/g) suggests that the observed activity is a result of the active sites at the interlayer space. In line with this view, an SEM image (Figure 2b) shows that the surface of spent $K_{0.8}Zn_{0.4}Ti_{1.6}O_4$ was roughened and the crystals expanded, in comparison to the dense crystals of as made $K_{0.8}Zn_{0.4}Ti_{1.6}O_4$ with a smooth surface. We propose that as made $K_{0.8}Zn_{0.4}Ti_{1.6}O_4$ intercalates palmitic acid vapor, as it does in the liquid phase. The intercalated palmitic acid and the reaction products might exert appreciable mechanical stress to the layers sandwiching them, such that the layers are deformed and then the crystals expanded. However, the preservation of the crystal structure and the associated two-dimensionality is clearly beneficial.

Conclusions

The surface and interlayer basic characters in lepidocrocite titanate $K_{0.8}Zn_{0.4}Ti_{1.6}O_4$ was investigated. $K_{0.8}Zn_{0.4}Ti_{1.6}O_4$ is a weak base as evaluated by CO_2 TPD. Besides, the low basicity implies the major contribution from O^{2-} sites at the external surfaces, while those at the interlayer region are not accessible to CO_2. Yet, the liquid-phase adsorption study suggests the intercalation of palmitic acid into the interlayer region as palmitate salts. The accessibility of interlayer basic sites in $K_{0.8}Zn_{0.4}Ti_{1.6}O_4$ was further demonstrated by its use as a catalyst in the gas phase ketonization of palmitic acid. Despite of small (external) surface area and low basicity, this lepidocrocite titanate was active and selective for the conversion of palmitic acid to hydrocarbons via ketonization-cracking. The layered structure was also preserved in contrast to other 2D basic catalysts reported so far. Moreover, the catalytic activity of lepidocrocite titanate can be tuned by the variation of the metal M^{I} and M^{II} substituting at Ti^{IV} sites.

Acknowledgements

The financial support from the Thailand Research Fund to T.M. (TRG5780160) and T.S. (BRG5680007) is acknowledged. The ^{1}H ultra-fast MAS NMR experiments were supported by the Natural Science Center for Basic Research and Development, Hiroshima University.

Supplementary Material: PXRD patterns and additional material and methods available

Reference

[1] Hattori, H. *J. Jpn. Petrol. Inst.*, **2004**, *47*, 67-81.
[2] Barthomeuf, D. *Catal. Rev. Sci. Eng.*, **1996**, *38*, 521-612.
[3] Ono, Y. *J. Catal.*, **2003**, 216, 406-415.
[4] Weitkamp, J.; Hunger, M.; Rymsa, U. *Microporous Mesoporous Mater.*, **2001**, *48*, 255-270.
[5] Lee, D. –W. ; Park, Y. –M.; Lee, K. –Y. *Catal. Survey Asia*, **2009**, *13*, 63-77.
[6] Chen, L.; Zhao, J.; Yin, S. –F.; Au, C. –T. *RSC Adv.*, **2013**, *3*, 3199-3814.
[7] Debecker, D. P.; Gaigneaux, E. M.; Busca, G. *Chem. Eur. J.*, **2009**, *15*, 3920-3935.
[8] Ma, R.; Sasaki, T. *Acc. Chem. Res.*, **2015**, *48*, 136-143.
[9] Cordeiro, C. S.; da Silva, F. R.; Marangoni, R.; Wypych, F.; Ramos, L. P. *Catal. Lett.*, **2012**, 142, 763-770.
[10] Cordeiro, C. S.; Arizaga, G. G. C.; Ramos, L. P.; Wypych, F. *Catal. Commun.*, **2008**, *9*, 2140-2143.
[11] Groult, D.; Mercey, C.; Raveau, B. *J. Solid State Chem.*, **1980**, *32*, 289-296.
[12] Reid, A. F.; Mumme, W. G.; Wadsley, A. D. *Acta Cryst.* **1968**, *B24*, 1228-1233.
[13] Gao, T.; Fjellvåg, H.; Norby, P. *Chem. Mater.*, **2009**, *21*, 3503-3513.
[14] Gao, T.; Norby, P.; Okamoto, H.; Fjellvåg, H. *Inorg. Chem.*, **2009**, *48*, 9409-9418.
[15] England, W. A.; Birkett, J. E.; Goodenough, J. B.; Wiseman, P. J. *J. Solid State Chem.*, **1983**, *49*, 300-308.
[16] Gao, T.; Fjellvåg, H.; Norby, P. *J. Mater. Chem.*, **2009**, *19*, 787-794.
[17] Song, H. Y.; Sjastad, A. O.; Vistad, O. B.; Gao, T.; Norby, P. *Inorg. Chem.*, **2009**, *48*, 6952-6959.
[18] Sasaki, T.; Kooli, F.; Iida, M.; Michiue, Y.; Takenouchi, S.; Yajima, Y.; Izumi, F.; Chakoumakos, B. C.; Watanabe, M. *Chem. Mater.*, **1998**, *10*, 4123-4128.
[19] Sasaki, T.; Watanabe, M.; Michiue, Y.; Komatsu, Y.; Izumi, F.; Takenouchi, S. *Chem. Mater.*, **1995**, *7*, 1001-1007.
[20] Grey, I. E.; Li, C.; Madsen, I. C.; Watts, J. A. *J. Solid State Chem.*, **1987**, *66*, 7-19.
[21] Kitano, M.; Nakajima, K.; Kondo, J. N.; Hayashi, S.; Hara, M. *J. Am. Chem. Soc.*, **2010**, *132*, 6622-6623.
[22] Draskovic, T. I.; Wang, T.; Henderson, C. N.; Mallouk, T. E. *Int. J. Hydrogen Energy*, **2014**, *39*, 4576-4580.
[23] Fukuda, K.; Akatsuka, K.; Ebina, Y.; Ma, R.; Takada, K.; Nakai, I.; Sasaki, T. *ACS Nano*, **2008**, *2*, 1689-1695.
[24] Maluangnont, T.; Matsuba, K.; Geng, F.; Ma, R.; Yamauchi, Y.; Sasaki, T. *Chem. Mater.*, **2013**, *25*, 3137-3146.
[25] Sasaki, T.; Watanabe, M. *J. Am. Chem. Soc.*, **1998**, *120*, 4682-4689.
[26] Gaertner, C. A.; Serrano-Ruiz, J. C.; Braden, D. J.; Dumesic, J. A. *J. Catal.*, **2009**, *266*, 71-78.
[27] Deng, L.; Fu, Y.; Guo, Q. X. *Energy Fuels*, **2009**, *23*, 564-568.
[28] Pham, T. N.; Sooknoi, T.; Crossley, S. P.; Resasco, D. E. *ACS Catal.*, **2013**, *3*, 2456-2473.
[29] Renz, M. *Eur. J. Org. Chem.* **200**5, 979-988.
[30] Climent, M. J.; Corma, A.; Iborra, S.; Epping, K.; Velty, A. *J. Catal.*, **2004**, *225*, 316-326.
[31] Grigorieva, A. V.; Yuschenko, V. Y.; Ivanova, I. I.; Goodilin, E. A.; Tretyakov, Y. D. *J. Nanomater.*, **2012**, 920483.
[32] Santos-Lopez, I. A.; Handy, B. E.; Garcia-de-Leon, R. *Thermochimica Acta* **2013**, *567*, 85-92.
[33] Raupp, G. B.; Dumesic, J. A. *J. Phys. Chem.*, **1985**, *89*, 5240-5246.
[34] Hu, W.; Li, L.; Li, G.; Liu, Y.; Withers, R. L. *Sci. Rep.* **2014**, *4*, 6582.

[35] Izawa, H.; Kikkawa, S.; Koizumi, M. *J. Phys. Chem.*, **1982**, *86*, 5023-5026.
[36] Sasaki, T.; Watanabe, M.; Komatsu, Y.; Fujiki,Y. *Inorg. Chem.*, **1985**, *24*, 2265-2271.
[37] Sasaki, T.; Komatsu, Y.; Fujiki, Y. *Chem. Mater.*, **1992**, *4*, 894-899.
[38] Markovits, A.; Fahmi, A.; Minot, C. *J. Mol. Struct. Theochem* **1996**, *371*, 219-235.
[39] Takagaki, A.; Sugisawa, M.; Lu, D.; Kondo, J. N.; Hara, M.; Domen, K.; Hayashi, S. *J. Am. Chem. Soc.*, **2003**, *125*, 5479-5485.
[40] Yu, G.; Zhou, Y.; Yang, R.; Wang, M.; Shen, L.; Li, Y.; Xue, N.; Guo, X.; Ding, W.; Peng, L. *J. Phys. Chem. C*, **2015**, *119*, 12325-12334.
[41] Bavykin, D. V.; Carravetta, M.; Kulak, A. N.; Walsh, F. C. *Chem. Mater.*, **2010**, *22*, 2458-2465.
[42] Corcoran, D. J. D.; Tunstall, D. P.; Irvine, J. T. S. *Solid State Ionics* **2000**, *136-137*, 297-303.
[43] Maluangnont, T.; Bui, G. T.; Huntington, B. A.; Lerner, M. M. *Chem. Mater.*, **2011**, *23*, 1091-1095.
[44] Maluangnont, T.; Sirisaksoontorn, W.; Lerner, M. M. *Carbon* **2012**, *50*, 597-602.
[45] Nakano, S.; Sasaki, T.; Takemura, K.; Watanabe, M. *Chem. Mater.*, **1998**, *10*, 2044-2046.
[46] Fujimoto, K.; Tobito, N.; Ito, S. *J. Ion Exchange* **2015**, *25*, 12-15.
[47] Shirpour, M.; Cabana, J.; Doeff, M. *Chem. Mater.*, **2014**, *26*, 2502-2512
[48] Sasaki, T.; Izumi, F.; Watanabe, M. *Chem. Mater.*, **1996**, *8*, 777-782
[49] Arizaga, G. G. C.; Mangrich, A. S.; da Costa Gardolinski, J. E. F.; Wypych, F. *J. Colloid Interface Sci.*, **2008**, *320*, 168-176.
[50] Chou, C. –C.; Chiang, M. –L.; Lin, J. –J. *Macromol. Rapid Commun.* **2005**, *26*, 1841-1845.
[51] Kandare, E.; Hossenlopp, J. M. *Inorg. Chem.*, **2006**, *45*, 3766-3773.
[52] Parida, K.; Das, J. *J. Mol. Catal. A* **2000**, *151*, 185-192.
[53] Das, J.; Parida, K. *React. Kinet. Catal. Lett.* **2000**, *69*, 223-229.

Highlights

- $K_{0.8}Zn_{0.4}Ti_{1.6}O_4$ intercalates palmitic acid, forming the occluded potassium salt.
- The interlayer expansion is evidenced by PXRD patterns and TEM image.
- Two types of basic sites are deduced from ultrafast ^{1}H MAS NMR
- Lepidocrocite titanate catalyses ketonization of palmitic acid to palmitone and corresponding cracked products.

Graphical Abstract Legend

Interlayer basic sites in lepidocrocite titanate, $K_{0.8}Zn_{0.4}Ti_{1.6}O_4$, lead to an intercalation of palmitic acid with a layer expansion.